UCRL-17521

University of California

Ernest O. Lawrence Radiation Laboratory

LOW-TEMPERATURE DISLOCATION MECHANISMS

Berkeley, California

DISCLAIMER

Prepared for presentation at the
Battelle Colloquium on Dislocation Dynamics
Seattle, May 1 - 5, 1967

UCRL-17521
Preprint

UNIVERSITY OF CALIFORNIA

Lawrence Radiation Laboratory
Berkeley, California

AEC Contract No. W-7405-eng-48

LOW-TEMPERATURE DISLOCATION MECHANISMS

John E. Dorn

April, 1967

UCRL-17521

LOW-TEMPERATURE DISLOCATION MECHANISMS

John E. Dorn

Inorganic Materials Research Division, Lawrence Radiation Laboratory, and the Department of Mineral Technology, College of Engineering, University of California, Berkeley, California

April 1967

INTRODUCTION

The objectives of this paper are (1) to place in perspective the present status of knowledge on the plastic behavior of metals and alloys, (2) to point out some of the weaknesses in current theories, and (3) to suggest some interesting areas for future research. In order to confine this presentation to tractable dimensions, certain important and very interesting topics, such as mechanisms for strain hardening and mechanisms for high temperature diffusion-controlled flow, etc., will not be discussed. Even for the low-temperature mechanisms that will be emphasized here, it will not be possible to recount all details of interest. Condensation of this vast subject will be accomplished by adopting a simple classification of dislocation mechanisms that will provide a frame of reference within which the details for different mechanisms of the same class involve only variations on the same theme.

CLASSIFICATION OF DISLOCATION MECHANISMS

The yield strength of imperfect crystals is determined by the resolved shear stress that is needed to move glide dislocations across their slip planes. If there were no obstacles present, dislocations would sweep through crystals at infinitesimally low stresses. All real crystals, however, contain obstacles. It is the nature and distribution of such obstacles that determines the plastic behavior of metals and alloys.

The fact that glide dislocations are line imperfections that move on slip planes of a three-dimensional crystal demands that the obstacles they encounter must perforce also have geometrical characteristics. Consequently obstacles might be classified as localized, linear, and volumetric as suggested in the first column of Table 1. Typical examples of each major type of obstacle are listed in the third column: (1) Localized obstacles serve to arrest dislocations over limited lengths between which the dislocations bow out under applied stresses. (2) Linear obstacles arrest entire dislocation segments along a line. (3) Volumetric obstacles involve energy dissipative mechanisms arising from interactions of stress fields of moving dislocations with various lattice phenomena over the volume of the lattice.

The virtue of the proposed classification extends beyond its geometrical origin: Although each major class of obstacles exhibits somewhat different dislocation mechanisms, individual mechanisms within one class have a common basis. Distinctions between mechanisms in any one class appear as interesting variations of a common theme. Mechanisms need be classified, not only in terms of the geometry of the obstacles that dislocations must bypass or surmount, but also relative to their response to thermal fluctuations: Thermally activated mechanisms are facilitated by thermal fluctuations in energy whereas athermal mechanisms are much more highly resistant to the effects of such fluctuations. All mechanisms are athermal at the absolute zero of temperature since, here, the probability for any thermal fluctuation is zero. By their very nature as volumetric

energy dissipative processes for moving dislocations, Class III mechanisms are intrinsically athermal and remain so under all environmental conditions. These mechanisms suggest that the velocity, v, of a dislocation is linearly related to the force τb acting on the dislocation according to

$$v = B\tau b$$

where τ is the applied stress, b the Burger's vector and B is the mobility.

Mechanisms of Class I and Class II can be further grouped into two major subclasses, thermally-activatable and athermal mechanisms. Thermally activatable mechanisms are those in which thermal fluctuations can assist the applied stress in nucleating the forward motion of a segment of the dislocation. Each unit event in a thermally activated process takes place with a frequency dictated by the Boltzmann expression, namely,

$$\nu' = \nu\, e^{-\frac{U\{\tau,\ \text{structure},\ T\}}{kT}} \qquad (2)$$

where ν is a fundamental frequency of the mechanism in question, U is the additional energy that need be supplied by a thermal fluctuation to cause the dislocation to surmount the obstacle and kT, is the Boltzmann constant times the absolute temperature. The applied stress does work on the dislocation as it surmounts an obstacle so that the energy U that must be supplied by a thermal fluctuation decreases as the applied stress is increased. The activation energy is always mildly sensitive to T as dictated by the variation of the

shear modulus of elasticity and therefore U varies with temperature. For the localized obstacle mechanisms, U also depends on substructural details. The frequency of the reverse reaction, is negligibly small at low temperatures because excessively high thermal fluctuations would be required to move dislocations against the force acting on them due to the applied stress. The plastic shear strain rate, $\dot{\gamma}$, for a single isolated thermally activated mechanism is given by the well-known expression

$$\dot{\gamma} = NAb\nu' = NAb\nu\, e^{-\frac{U}{kT}} \qquad (3)$$

where N is the number of points per unit volume where thermal fluctuations can stimulate nucleation of slip, and A is the average area swept out by the dislocation per successful event. The terms N, A, and ν also depend on the details of the mechanism. Thermally activated mechanisms are characterized by a rapidly decreasing stress with increasing temperature for constant strain-rate tests, and by an increasing stress with increasing strain rate for constant temperature tests.

Athermal mechanisms of Class I and Class II fall into two groups. One group is inherently athermal since the energy for nucleating forward slip never reaches a maximum value. This occurs in short-range order hardening. As a segment of a dislocation in a short-range ordered alloy bows out the energy continuously increases due principally to the disordering that is induced across the slip plane. For this type of mechanism therefore deformation must be induced

exclusively mechanically by a sufficiently high stress to cause disordering. Here the yield stress is insensitive to the strain rate and decreases with increasing temperature proportional to the product of the degree of order and the ordering energy. At high temperatures, however, fluctuations in short range order take place by diffusional processes which permit local advances of the dislocation and thus lead to thermally activated creep. But this subject is beyond the intended scope of the present report. A second group of mechanisms is environmentally athermal. Typical examples are the surmounting of long range stress fields and the breaking of attractive junctions. These mechanisms are inherently thermally activatable since the energy to surmount such obstacles has a maximum value. But at low temperatures and stresses, thermal fluctuations of sufficient energy are so infrequent, that they are ineffectual in assisting the nucleation process. Consequently deformation here must be induced almost exclusively by mechanical means, and therefore the yield stress is insensitive to the strain rate and it decreases very modestly with increasing temperature proportionally to the shear modulus of elasticity. The breaking of attractive junctions etc. are, however, thermally activatable at higher stresses and temperatures.

Some mechanisms are thermally activatable under some conditions and athermal under others. For example, dilute and weak Cottrell-atmosphere solute-atom locked dislocations are thermally activatable; but more concentrated and stronger Cottrell-atmosphere solute-atom locked dislocations are athermal and in many instances the

dislocations are so tightly bound that they cannot be torn away from their atmosphere even at very high stresses. Suzuki locking constitutes a second example: Weak Suzuki locking of partials having a narrow stacking fault ribbon are thermally activatable but under otherwise similar conditions, in alloys that have low stacking fault energies, the unlocking mechanism is athermal. The transition of Cottrell locking from a thermally activatable to an athermal mechanism is principally due to the height of the activation energy barrier whereas this transition for Suzuki locking arises from the fact that high thermal fluctuations in energy can only occur over small volumes of the crystal.

An example of some of the types of phenomena that are observed is illustrated by the experimental data summarized in Fig. 1a.[58] Over the low temperature range (I_T) a thermally activated mechanism, namely intersection of dislocations, is observed. Above T_c an athermal mechanism that is insensitive to temperature and strain rate is operative. Although the details of the athermal mechanism are yet under discussion it must in large measure consist of bowing out of dislocations from entanglements,[59,60] breaking of attractive junctions,[21-23] and perhaps surmounting some long range stress fields.

The stress at the absolute zero for the thermally activated range represents that needed to surmount obstacles without aid from thermal fluctuations. At yet higher stresses, Class III types of viscous athermal mechanisms, Fig. 1b, are the only ones that remain

effective for determining the velocity of dislocations and the strain rate.[61]

The major objectives of investigations on dislocation mechanisms are (1) to provide a basic understanding of the varied plastic behavior metals and alloys undertake, (2) to so formulate plastic behavior to permit these concepts to be utilized in engineering applications and (3) to provide a basis for development of new and superior alloys having special desirable properties. The achievement of even the first objective is a major undertaking primarily because, a number of mechanisms of each Class of Table 1 is always simultaneously operative. Furthermore in many instances it is not always clear how the effects of several mechanisms might be satisfactorily treated in a unified way. Only the most modest introduction[62] of statistics has been attempted for simple cases of single mechanisms in spite of the fact that the need for statistical approaches is so obvious. On the basis of the inherent complexity of the whole problem it is indeed remarkable that any progress could have been made. Fortunately, for certain restrictive conditions and over limited ranges of conditions, one identifiable mechanism often seems to predominate. Before discussing these issues it will be necessary to first describe and characterize prototype examples of each of the two classes of thermally activated mechanisms and some of their interesting variants.

CUTTING LOCALIZED OBSTACLES

A prototype example for cutting localized obstacles is given by

Seeger's approximation for the intersection mechanism.[5] Statistics are neglected and the obstacles are assumed to form a regular "square" array (subscript "s") of ℓ_s on a side as shown in Fig. 2a. Under a resolved shear stress τ_s^* the dislocations contact obstacles and arc out between them as given by $\tau_s^* = \Gamma/bR$ where Γ is the average line energy and R is the radius of curvature. Consequently a force F_s acts on the obstacle, which is assumed to be rigid. For the present the force-displacement diagram for cutting of Fig. 2b will be assumed, where the strength of the obstacle is given in terms of the line energy, Γ, times a strength factor, α, namely $F_{sc} = \alpha\Gamma$. If $F_s \geq \alpha\Gamma$ the obstacle will be cut athermally; but when $F_s \leq \alpha\Gamma$, cutting will take place only with the aid of a thermal fluctuation in energy of magnitude $U = \alpha\Gamma D - \tau_s^* b\ell_s D$ or greater. Then by Eq. (3)

$$\dot{\gamma} = \frac{\rho}{\ell_s}\,\ell_s^2 b\left(\frac{\nu_o b}{\ell_s}\right) e^{-\frac{(\alpha\Gamma D - \tau_s^* b\ell_s D)}{kT}} \qquad (4)$$

where $N \simeq \rho/\ell_s$, ρ being the density of glide dislocations, $A \simeq \ell_s^2$ and $\nu \simeq \nu_o\, b/\ell_s$ where ν_o is the Debye frequency.

If, following Seeger's approach, it be assumed that the athermal behavior arises exclusively from long range stress fields of dislocations, a very simple analysis is obtained: Let, for example the long range stress fields exhibit a maximum average amplitude τ_G over a fraction f of the slip plane. Then the effective stress promoting thermal fluctuations is given by $\tau_s^* = \tau_s - \tau_G$ where τ_s is the externally

applied stress, and the dislocations will glide freely over the fraction 1 - f of the slip plane. On this basis Eq. (4) reduces to

$$\tau_s = \tau_G + \frac{\alpha\Gamma D}{b\ell_s D} - \frac{kT}{b\ell_s D} \ell n \frac{\rho b^2 \nu_o}{f\dot{\gamma}} \qquad 0 \leq T \leq T_c \tag{5a}$$

$$\tau_s = \tau_G \qquad T_c \leq T \tag{5b}$$

where T_c defined by

$$\alpha\Gamma D = kT_c \ell n \frac{\rho b^2 \nu o}{f\dot{\gamma}} \tag{5c}$$

is the critical temperature above which thermal fluctuations in energy greater than $\alpha\Gamma D$ occur as frequently as is needed to maintain the imposed strain rate even when $\tau^* \approx 0$.

To this approximation the mechanical behavior for cutting a simple type of localized obstacle might be interpreted as shown in Fig. 3. The stress to induce flow at the absolute zero is given by $\tau_o = \tau_{G_o} + \alpha\Gamma_o/b\ell_s$ and increases with τ_{G_o} and the reciprocal of the mean spacing of obstacles, namely $1/\ell_s$. The effects of $\dot{\gamma}$ and T on τ (Fig. 3a) appear to agree, at least qualitatively, with the experimental data recorded in Fig. 1.

On the basis of this model higher strength alloys might be made in the following ways: (1) By increasing τ_G which uniformly elevates the τ - T curve, (2) by increasing the density of obstacles i.e. decreasing ℓ_s (fig. 3b). If only this is done strengthening will be

limited to temperatures below T_c, (3) by introducing stronger obstacles, i.e. increasing α (Fig. 3c). For this case the strengthening is extended to higher temperatures since T_c is linearly related to α. But when α is increased above 2, dislocations will bow through obstacles athermally by the Orowan process[24] at about the stress $\tau_B = \Gamma/bR = 2\Gamma/b\ell_s$ thus limiting the maximum achievable stress at low temperatures, as shown in Fig. 3c.

VARIATIONS FROM THE IDEALIZED PROTOTYPE

Rarely do Eqs. (5) depict the experimentally observed trends with satisfactory accuracy. Four factors serve to contribute to deviations from the idealized case: (1) Usually the force-displacement diagram differs from the simple case assumed in Fig. 2b. (2) Obstacles never form a regular array as assumed in Fig. 2a. Occasionally they are clustered as e.g. when forest dislocations in entanglements are cut. Usually they are more or less randomly distributed as in the case of tetragonal strain centers or Guinier-Preston zones. (3) Almost always several kinds of obstacles are present at one time. Even in the simple example of cutting forest dislocations in single crystals of pure f.c.c. and b.c.c. metals repulsive trees and attractive junctions need be considered simultaneously. (4) The interactions of the same obstacles with dislocations is often highly dependent on orientation, size and morphology of the obstacle and also on whether the dislocation be in screw or edge orientation as is the case for cutting through stress fields due to substitutional alloy strengthening.

Although these complexities do not change the general format of the approach to the cutting mechanisms that was given in the preceding section, they modify, and often drastically so, the expected trends.

A. Force-Displacement Diagrams for Cutting Localized Obstacles

The force-displacement diagram for cutting localized obstacles shown in Fig. 2b is approximated only for the simple case of intersection of undissociated basal-glide dislocations in h.c.p. systems with unreactive forest dislocations. For all other types of obstacles more complicated diagrams are obtained. The case of cutting noninteracting undissociated forest dislocations by dissociated glide dislocations, will serve as an example: Before a pair of jogs can be produced, the dissociated glide dislocation must first be constricted, Fig. 4a. Although the details of how the constriction and jogging sections of the force-displacement diagram might be merged is not well known, the approximate representation given in Fig. 4b cannot be seriously in error. A crude line-energy model for the force-diaplacement diagram for constriction of modestly dissociated dislocations[63] suggests that

$$F_c \approx 2/3\ \Gamma \sqrt{1 - \left[1 - 0.18\left(\frac{-x}{x_o} + \ln \frac{x_o}{x_o - x}\right)\right]^2} \qquad x_o - x \geq b \qquad (6a)$$

$$F_c \approx 2/3\ \Gamma \sqrt{1 - \left[1 - 0.18\left(\frac{-x}{x_o} + 1 - \frac{x_o - x}{b} + \ln \frac{x_o}{b}\right)\right]^2} \qquad x_o - x \leq b \qquad (6b)$$

The force to produce two jogs is estimated to be

$$F_{2j} = \Gamma/\pi \tag{6c}$$

Consequently the force-displacement diagram for glide dislocations having an equilibrium dissociation of $x_o = 5b$ for cutting a repulsive forest dislocation is in Fig. 4b. Whereas the total energy, U_m is the total area under the curve, the energy, U, that must be supplied by a thermal fluctuation to cause cutting when a stress τ_s^* is applied is given by the cross-hatched area. Numerical integration of Fig. 4b gives Fig. 4c which illustrates that for these cases free energy of activation no longer decreases linearly with the stress τ_s^* as was the case for the simple prototype. The strain rate is given by,

$$\dot{\gamma} = \rho b^2 \nu_o \, e^{-\frac{U}{kT}} \tag{7}$$

which reveals that U increases linearly with T for given values of $\dot{\gamma}$ and ρ. Whereas $U = 0$ and τ_s^* has its maximum value τ_{sm}^* at the absolute zero of temperature, U has its maximum value of U_m, where $\tau_s^* = 0$, at a critical temperature T_c defined by

$$\dot{\gamma} = \rho b^2 \nu_o \, e^{-\frac{U_m}{kT_c}} \tag{8}$$

T_c increases linearly with U_m and logarithically with $\dot{\gamma}/\rho$. For tests at constant values of $\dot{\gamma}$ and ρ

$$U/U_m \simeq T/T_c \tag{9}$$

Consequently Fig. 4c represents a normalized τ_s^* - T curve for cutting a regular square distribution of localized obstacles for constant values of $\dot{\gamma}$ and ρ. The value of U_m can be determined from the experimental values of T_c for two strain rates according to

$$\frac{\dot{\gamma}_1}{\dot{\gamma}_2} = \frac{e^{-\frac{U_m\{T_{c1}\}}{kT_{c1}}}}{e^{-\frac{U_m\{T_{c2}\}}{kT_{c2}}}} \qquad (10)$$

where the bracketed terms designate that U_m should be corrected for the differences in the shear modulus of elasticity with temperature. The effects of modifications of the force-displacement diagram for cutting obstacles on the τ^* - T relationship is illustrated in Fig. 4c. Estimates of the force-displacement diagrams for cutting a wide variety of localized obstacles are now available.

B. Randomly-Distributed Localized Obstacles

Localized obstacles never present themselves in regular square arrays: Occasionally they are clustered as in the case of dislocation intersection when entanglements develop; nevertheless these obstacles, are somewhat randomly distributed in the entanglements. In other cases, e.g. the presence of tetragonal strain centers, the dispersion of localized obstacles approaches a random distribution. If a square array of obstacles gave trends that closely agreed with the more realistic random distribution the issue would be unimportant. But

enough progress has been made on statistical treatments of the problem to suggest that the differences are not always trivial.

As the applied stress is increased, dislocations bow to smaller radii of curvature causing the average link length, $\bar{\ell}$, between the obstacles to decrease. Friedel[62] estimated the effect of τ^* on $\bar{\ell}$ by assuming steady state cutting, such that for each obstacle that was cut the average area ℓ_s^2, Fig. 5, was swept out. For weak obstacles, $\bar{\ell}$ decreases with increasing τ^* according to

$$\bar{\ell} = R\, 2^{1/3} \left(\frac{\ell_s}{R}\right)^{2/3} = \left(\frac{2\Gamma\ell_s^2}{\tau^* b}\right)^{1/3} \qquad (11)$$

The athermal yield stress at the absolute zero, given by $\tau^* \bar{\ell}\, b = \alpha\Gamma$, for the Friedel statistical model is contrasted with that predicted for a square array in Fig. 5c. On the same graph are shown the points obtained from computerized experiments by Foreman and Makin[64] on cutting randomly distributed obstacles. The two approaches lead to similar results which reveal that the athermal flow stress for a random distribution of obstacles is substantially lower than that predicted for a square array.

The distribution of obstacles also has a pronounced influence on the τ^* - T relationship deduced for the thermally activated cutting mechanism. Both the average number of obstacles contacted by the dislocation, $N = \rho/\bar{\ell}$, and the average frequency of vibration, $\nu = \nu_o b/\bar{\ell}$, are functions of the stress for the random distribution. For weak obstacles the shear strain rate becomes

$$\dot{\gamma} = \left(\frac{\rho}{\ell}\right) \ell_s^2 \left(\frac{\nu_o b}{\ell}\right) e^{-\frac{U}{kT}} = \frac{\rho \nu_o b^2}{2^{2/3}} \left(\frac{\tau^* b \ell_s}{\Gamma}\right)^{2/3} e^{-\frac{U}{kT}} \qquad (12)$$

where the average area swept out per activation is taken to be ℓ_s^2 and where the activation energy (assuming the force-displacement diagram of Fig. 2b) is given by

$$U = \alpha \Gamma D - \tau^* \bar{\ell} b D = \Gamma D \{\alpha - 2^{1/3} \left(\frac{\tau^* b \ell_s}{\Gamma}\right)^{2/3}\} \qquad (13)$$

The bracketed stress term in the preexponential expression of Eq. (12) demands that for any finite value of the strain rate, $\dot{\gamma}$, the stress τ^* can never be zero and therefore, in contrast to the square array model, T_c is infinite. A comparison, Fig. 6, of the τ^* - T relationship predicted by Friedel's model with that deduced for a square array of obstacles reveals the importance that must be ascribed to a consideration of the statistics of the problem: Randomly dispersed obstacles give much lower stresses over the lower temperature range than is obtained from square arrays. Over the higher temperature range, however, the stress, τ^*, for the random distribution of obstacles lies above that predicted for a square array model and decreases very slowly with increasing temperature.

Kocks[65] has recently presented a detailed statistical approach to the problem of cutting randomly distributed obstacles. His method of approach has been adopted by Guyot and Stephansky.[66] They consider an obstacle at O of Fig. 7 contacted by an originally straight dislocation AB. Under a stress τ^*, R makes an angle ϕ, with its

original configuration provided there are no obstacles in area A_1 and some in dA_1. The force on the central obstacle is given by Eq. (16) and reaches the cutting force at a critical value of ϕ_c, given by Eq. (17), where ϕ_c is the complement of $\psi_c/2$. The important feature is that the force on the obstacle does not depend directly on the length ℓ_s, as assumed in the square array model and not on the average link length, $\bar{\ell}$, as assumed by Friedel, but rather on the angles ϕ_1 and ϕ_2. Therefore the probability that an obstacle will be cut is equal to the probability there are no obstacles in A_1 and A_2 or any larger area when $(\phi_1 + \phi_2)/2$ exceeds ϕ_c. The probability that there are no obstacles in A_1 and A_2 is given by the well-known expression $P = \exp - \{(A_1 + A_2)/\ell^2_s\}$. The probability for cutting an obstacle, P_c, deduced from this approach is given in Fig. 8 as a function of $\ell_s/R = \tau^* b\ell_s/\Gamma$. Obstacles for which $\alpha > 2$, are not cut but may be by-passed by the Owowan mechanism.

Whereas it was assumed that a single cutting would permit the dislocation to move only over the average area ℓ_s^2 in the square array and Friedel's models, it has been demonstrated, by Kocks and by the computerized experiments of Foreman and Makin, that a larger area is swept out. This arises because once a cutting has been achieved there is a certain probability the dislocation can unzip past the next neighbors etc. An approximate calculation suggests that the area swept out per cutting is given by

$$A_i = \frac{i\ell_s^2}{i - jP_c} \qquad (18)$$

where i equals one, plus the number of obstacles that were cut by unzipping, and j is the number of new obstacles contacted by an advance of the so-released dislocation segment. Since j is greater than unity, A_1 becomes infinite at some critical stress. This stress is conveniently defined as the athermal yield stress. Detailed analyses have shown that i and j depend on the stress. The calculated values of jP_c, where yielding takes place, are also recorded in Fig. 8. These data provide the basis for determining the athermal yield stress. The results agree well with Foreman and Makins curve, Fig. 5, up to $\alpha \approx 1.2$ and fall somewhat below this curve for yet higher values of α.

These results emphasize the need for more complete and accurate statistical treatments for cutting localized obstacles.

C. Effects of Additional Factors

The general problem of plastic deformation arising from cutting of localized obstacles is complicated by the intrusion of several factors. One concerns the fact that almost invariably several kinds of obstacles having quite different force-displacement diagrams are present simultaneously.

The original concept on intersection in single crystals of pure f.c.c. metals suggested that their plastic behavior could be ascribed to the cutting of repulsive trees imbedded in a long range internal stress field. Under these circumstances the Seeger's superposition principle that $\tau = \tau^* + \tau_G$ is applicable; but only τ can be measured directly and it is often difficult to separate accurately

τ^* from τ_G. Furthermore, when Seeger's superposition principle is applied, special assumptions are required in order to account for the observed constancy of the Cottrell-Stokes[67] ratio over Stages II and III.

An alternate suggestion has been made that the crystal cannot support long range stress fields due to relaxation of stresses by motion of dislocations on secondary slip planes.[68] It has therefore been proposed that intersection involves principally the cutting of repulsive trees and attractive junctions, the long range stress fields being negligibly small and the attractive junction cutting being largely responsible for the apparent athermal behavior. It is obvious that in this event the Seeger's superposition principle cannot be applied with rigor. The yield stress over the higher temperature range will yet be influenced by the presence of some repulsive trees located near the attractive junctions and will thus affect the apparent athermal stress level. Furthermore, such an apparent athermal stress level, τ_A, cannot be extrapolated into the lower temperature range to give a meaningful $\tau^* = \tau - \tau_A$ because if the weaker repulsive trees are not instantly penetrable, most of the stronger attractive junctions must yet remain unbroken. In fact, in this model, the motion of glide dislocations must proceed first by thermally activated cutting some of the repulsive trees which then releases sufficiently long dislocation segments to facilitate activated cutting of attractive junctions. A simple non-statistical model for this mechanism, reveals that the predicted trends of τ versus T

for the repulsive tree-attractive junction model do not differ greatly from that for the repulsive tree-long range stress field model. Furthermore the Cottrell-Stokes ratio is inherent to the model. On the other hand the interpretation of the data are uniquely different for each of the two possibilities.

Because entanglements form so as to lower the energy of the crystal, it follows that thermally activated cutting of repulsive trees as well as attractive junctions probably involves motion of the dislocation against the attractive stress field of the entire entanglement. This effect introduces an athermal long range stress component that warrants additional detailed consideration.

Rather good progress has been made in qualitatively rationalizing some of the effects of solute atoms,[7-12] tetragonal defects,[9-12] precipitates and dispersed phases[15,16,24-26] on the yield strengths of alloys. Inasmuch as no major advance has been made in these areas since they were last summarized, details will not be reviewed here again. It is appropriate, however, to reconsider the validity of some of the simplifications that have been made to facilitate analyses. Although some improvement in the accuracy of the force-displacement diagrams for cutting stress fields due to isolated strain centers is needed, the major issues seem to be concerned more with the statistical features of the problem. The stress fields due to lattice strain centers decrease very rapidly in height spread over larger areas of the slip plane as their distance from the slip plane increases. It has therefore been customary to neglect the effects of all strain centers

lying a greater distance away than one atomic plane on either side of the slip plane. On this basis $\ell_s \simeq b/\sqrt{2c}$ where c is the concentration of strain centers. In a number of examples[11] there is experimental confirmation of this simplification relative to the variation of τ^* with $\sqrt{c}$. At higher temperatures and therefore correspondingly lower values of τ^*, however, the weaker and broader stress fields of more distant strain centers must be felt by the dislocations. The very difficult statistics of this problem has been almost completely neglected. Superposition of stress fields due to clusters of strain centers near the slip plane can give rise to local regions having quite different force-displacement diagrams from those of the isolated centers. Clusters more remotely displaced from the slip plane, can contribute to long-range stress field interactions with dislocations. Coupled with these issues is the further need for considering the effects of dislocations-localized obstacle interactions on the preexponential expression in the strain-rate equation. In terms of these comments it is quite understandable why the radiation damage problem[17-20] is so difficult to cope with in detail.

In general the presence of repulsive trees, and attractive junctions have been neglected in problems of alloy strengthening. For cases of strong tetragonal strain centers where $c \geq 10^{-7}$ this omission is justified over the lower temperature range of the thermally activated region since the distance ℓ_s between the repulsive trees and attractive junctions is much greater than that for the strain centers. Nevertheless the presence of attractive junctions should have significant effects on

the yield stress at higher temperatures.

The problem is somewhat more complicated for isotropic strain centers (e.g. substitutional alloy strengthening) since they interact appreciably only with the edge components of dislocations. Thus the motion of screw components is effectively resisted only by forest dislocations whereas the edge components are held up principally by the stress fields of the isotropic strain centers. No theory has yet been formulated that takes these issues into consideration. Furthermore, alloying often alters the stacking fault energy and thus modifies the force-displacement diagrams for cutting trees. In addition tendencies toward short-range ordering or clustering influence the athermal stress level. These individual factors are not easily isolated experimentally. There is indeed need for a comprehensive theory that takes these significant factors pertaining to substitutional solid solution strengthening into detailed consideration.

LINEAR OBSTACLES

A. Prototype Model

The Peierls mechanism will serve as the prototype model for thermal activation of dislocation motion past linear obstacles. A rather complete review of this mechanism[35] has been given recently and therefore only the major features need be presented here to provide the basis for discussion.

The energy of a dislocation line is least when it lies parallel to rows of atoms on the slip plane (Fig. 9). As it moves from one

valley to the next the core energy and thus the line energy changes periodically as shown. The Peierls stress τ_p is that which is required to push the dislocation mechanically past the steepest part of the hill whereupon it will advance from one valley to the next, etc. Thus τ_p is the yield stress at the absolute zero. Under a stress $\tau^* < \tau_p$ the dislocation will move part way up the hill to A_1 A_2. At the absolute zero no further motion can take place. But at higher temperatures thermal fluctuations in energy can push the dislocation locally (e.g. B of Fig. 9) toward the next valley. The fluctuation in energy needed to nucleate a pair of kinks is due to the increased energy of the now longer dislocation line less the work supplied by the stress τ^* in sweeping out the additional area. For a sufficiently vigorous fluctuation, (e.g. D of Fig. 9) the energy reaches a maximum value. All fluctuations in energy equal to or greater than this value will nucleate a pair of kinks. These then move apart under the action of the applied stress, thereby advancing the dislocation segment of length, ℓ, a distance a to the next valley in the slip plane. The energy required to nucleate in this way a pair of kinks U_n divided by twice the energy of a single complete kink, U_k, is a simple function of τ^*/τ_p, as shown in Fig. 9 b. A simple line energy calculation shows that the kink energy is given by

$$\frac{2\pi U_K}{a\Gamma_o} = 5.7 \left(\frac{\tau_p ab}{\pi \Gamma_o}\right)^{1/2} \qquad (19)$$

illustrating that the line energy of a dislocation can be deduced from experimental determination of the Peierls stress and the kink energy.

The strain rate is readily formulated as

$$\dot{\gamma} \simeq \left(\frac{\rho}{\ell}\right)(\ell a)\, b \left(\frac{\nu_o b}{w}\right)\left(\frac{\ell}{2w}\right) e^{-\frac{U_n}{kT}} = \frac{\rho \ell a b^2 \nu_o}{2w^2} e^{-\frac{U_n}{kT}} \tag{20}$$

where $\left(\frac{\rho}{\ell}\right)$ are the number of segments of dislocations that can be activated, (ℓa) is the area swept out, $\left(\frac{\nu_o b}{w}\right)$ is the frequency of vibration of a critical loop (Fig. 9a) and $(\ell/2w)$ are the number of segments along ℓ at which nucleation can take place. The quantity w has been shown to be almost independent of τ^* and can be approximated by

$$w \simeq \frac{\pi}{2}\left(\frac{2a\Gamma_o}{b\tau_p}\right)^{1/2} \tag{21}$$

As T increases, U_n increases and reaches a value of $2U_k$ at T_c where $\tau^*/\tau_p = 0$, whence

$$\dot{\gamma} = \frac{\rho \ell a b^2 \nu_o}{2w^2} e^{-\frac{2U_k}{kT_c}} \tag{22}$$

Consequently for a given strain rate

$$\frac{U_n}{2U_k} = \frac{T}{T_c}\frac{G_c}{G} \tag{23}$$

where G_c/G merely correct for the change in the shear modulus of

elasticity with temperature. The kink energy can be deduced by determining T_c for two different strain rates, namely

$$\frac{\dot{\gamma}_1}{\dot{\gamma}_2} = \frac{e^{-\frac{2U_k}{kT_{c1}}}}{e^{-\frac{2U_k}{kT_{c2}}}} \tag{24}$$

The experimentally determined activation volume is

$$v_a = kT \left\langle \frac{\partial \ell n \dot{\gamma}}{\partial \tau^*} \right\rangle_T = kT \left\langle \frac{\partial \ell n(\rho \ell)}{\partial \tau^*} \right\rangle_T - \left\langle \frac{\partial U_n}{\partial \tau^*} \right\rangle_T \tag{25}$$

where the theoretical activation volume (Fig. 9c) is given by

$$-\left(\frac{\partial U_n}{\partial \tau^*}\right) = v^* = \frac{-2U_k \, \partial\left(\frac{U_n}{2U_k}\right)}{\tau_p \, \partial\left(\frac{\tau^*}{\tau_p}\right)} \tag{26}$$

Thus far, all investigations that seem to confirm the Peierls mechanism have shown that $v_a \simeq v^*$.

A typical example of confirmation of the Peierls mechanism is given in Fig. 10 where it has been assumed that $\tau = \tau^* + \tau_A$. The experimental data are shown as points and the solid lines represent the theoretical curves. Whereas τ_p was deduced from the value of τ^* at 0°K, $2U_k$ was obtained from T_{c1} and T_{c2}. The line energy, deduced

from Eq. (19), is $\Gamma_o \simeq (2.5)\, Gb^2/2$, i.e. only slightly higher than the crude theoretical estimate. In addition other details for the model seem to be quite well satisfied.

B. Variants of the Prototype Linear Obstacle Model

Variants of the linear obstacle model differ from each other with respect to two features; namely the effect of stress on the activation energy and the effect of stress on the preexponential term in the strain rate expression. For example, Friedel's[37] well-formulated mechanism of slip resulting from cross slip of dissociated dislocations on the basal plane to perfect glide dislocations on the prism plane is illustrated in Fig. 11. On the basis of this model

$$\dot{\gamma} = \frac{NL_s Ab^4 \tau^{*2} \nu_o}{8\Gamma R_e} e^{-\frac{U_c}{kT}} e^{-\frac{2^{3/2}(\Gamma R_e^3)^{1/2}}{\tau^* bkT}} \tag{27}$$

where N is the number of screw segments of dislocations on the basal plane per unit volume each having a mean length L_s, A is the area swept out per activation, and

$$R_e \simeq \frac{\Gamma}{16} \ln \frac{x_o}{b} \tag{28a}$$

$$U_c \simeq \frac{\Gamma}{15} x_o \left(\ln \frac{x_o}{b}\right)^{1/2} \tag{28b}$$

where R_e is the recombination energy per unit length and U_c is the

constriction energy for an equilibrium separation, x_o, of the partial dislocations on the basal planes. This relationship is uniquely different from that for cutting localized obstacles and also that for the Peierls mechanism. Friedel's theory infers, in agreement with several experimental results, that when the resolved shear stress on the basal plane is zero, prismatic slip can only take place at rather high temperatures. As the temperature is decreased, the yield stress for prismatic slip increases rapidly and becomes infinitely high even somewhat above the absolute zero. However, the values of U_c and R_e can be reduced by the effects of shear stresses acting on blocked screw dislocations on the basal plane. This illustrates why prismatic slip may be observed in polycrystalline aggregates even at quite low temperatures.

C. General Comparisons

The above-mentioned formulation of Friedel's cross-slip mechanism has validity only when the two partials of the dissociated dislocation are distinctly separated. Eqs. (28a) and (28b) are no longer appropriate for cases where the stacking fault energy is so high that $x_o \approx 0.5$ to 2b. In this event it seems more appropriate to imagine that the core energy of a screw dislocation is decreased slightly by this minor separation of its partials rather than assuming that a true stacking fault is present. This strongly implies that before such a mildly dissociated screw dislocation can be moved on the prism plane of a h.c.p. metal its core energy must be increased

somewhat. Such a screw dislocation will then exhibit a periodic variation in energy as it is displaced from row to row of atoms in the prismatic plane. In this case the plastic behavior for prismatic slip can be expected to agree reasonably well with that for the Peierls mechanism where the ptoential energy hill may not be too dissimilar from the quasi-parabolic hill already analyzed by Guyot and Dorn.[35]

The above described psuedo-Peierls mechanism provides an acceptable interpretation of the effects of alloying with Li on the prismatic slip in Mg as illustrated in Fig. 12. There is an apparent transition from the Friedel cross-slip mechanism in pure Mg and Mg + 6 at.% Li to a Peierls type of mechanism for Mg + 10 at.% Li and Mg + 12 at.% Li suggesting that Li additions serve to increase the stacking fault energy in Mg.

There are three major points of difference between the true Peierls mechanism and the psuedo-Peierls mechanism; (1) Whereas the true Peierls mechanism applies to any dislocation in any orientation parallel to close-packed rows of atoms on the slip plane, the pseudo-Peierls mechanism applies only to dislocations in screw orientation that dissociate very little on secondary planes. (2) Whereas the true Peierls mechanism is expected to be operative in the early stages of straining some prestraining is required to place dislocations in screw orientation before the pseudo-Peierls mechanism can be controlling. The rate of strain hardening is expected to be high in the microstrain region. (3) Whereas the activation energy for the true Peierls mechanism should depend only on the shear stress on the

slip plane, that for the pseudo-Peierls mechanisms will depend also on the shear stresses on the secondary planes of dissociation.

The picture concerning the plastic behavior of b.c.c. metals at low temperatures is now rapidly being resolved. There are three principle schools of thought: One contends that the plastic behavior of b.c.c. metals arises from tetragonal strain centers due to interstitial impurities, a second that b.c.c. metals obey the Peierls mechanism and a third that their deformation is dependent on recombination of mildly dissociated dislocations, i.e. by a recombination mechanism. Although the validity of the first mentioned mechanism has been demonstrated experimentally in a number of other examples, it has not yet been shown that τ^* for b.c.c. metals increases linearly with $\sqrt{c}$ as should be the case if impurities were controlling the deformation. Furthermore it alone cannot account for the observed effects of orientation on yielding of b.c.c. metals. In many cases there is good experimental confirmation for the validity of the Peierls mechanism but again the effects of orientation cannot be explained on the basis of this mechanism alone. It currently appears that the recombination mechanism will eventually prove to be the most reliable because it can account for orientation effects, high initial rates of strain hardening and for any given orientation $\tau^* - T$ relationships that are Peierls-like. It is evident, however, that the more macroscopic formulation of the mechanism in terms of stacking-fault, recombination and constriction energies will have to be replaced by a more detailed atomistic picture of cores of slightly dissociated screw dislocations and the

changes in core configurations and energies under general states of stress.

The activation energy for cutting localized obstacles depends on the statistics of their distribution. In contrast that for nucleating slip past line obstacles is completely determined by the line configuration. Consequently the strain rate for dislocation motion past a series of different kinds of line obstacles depends essentially on the rate of nucleation past the most difficultly surmountable obstacle. Usually it is assumed that the superposition $\tau = \tau^* + \tau_A$ holds as it should if τ_A arises from long-range stress fields. Up to the present, however, that has been no adequate theoretical treatment of cases involving both localized and linear obstacles. On occasions the preexponential term is not strongly dependent on the stress (e.g. the Peierls mechanism) and then a finite T_c results for linear obstacles at which $\tau^* = 0$. But in other cases a finite T_c is not obtained either because of the stress dependency of the activation energy (e.g. cross slip) or the stress dependency of the preexponential term.

Table 1. Classification of Mechanisms

Types of Obstacles	Type of Mechanism	Representative Examples (incomplete listing)	Reference
1. Localized	Thermally activated cutting $\dot{\gamma} = \dot{\gamma}_o e^{-\frac{U}{kT}\{\tau^*, \text{struct.}, T\}}$ -U depends on statistics	Repulsive dislocation trees Solute atom stress fields Tetragonal strain centers Guinier-Preston zones	1 - 6 7 - 12 9 - 12 13 - 16
	Either or both	Radiation Damage Coherent precipitates Attractive junctions	17 - 20 15 - 16 21 - 23
	Athermal $\tau_G = \tau_{Go} G/G_o$	Incoherent precipitates Long Range stress fields	24 - 26 27 - 29

UCRL-17521

Table 1. Continued

2. Linear	Thermally activated $\dot{\gamma} = \dot{\gamma}_o e^{-\frac{U}{kT}\{\tau^*, T\}}$ U not dependent on statistics	Peierls mechanism Cross-slip Recombination Psuedo-Peierls Mechanism Cottrell-Lomer dissociation	30 - 35 36 - 37 38 39
	Either	Fisher unlocking Suzuki unlocking	40 41
	$\tau_A \equiv \tau_A$ (order)	Short Range Order Long Range Order	42 - 43 44
3. Volumetric	Athermal $\dot{\gamma} = \beta\tau$	Thermoelastic Phonon scattering Phonon viscosity Electron Viscosity	45 - 48 49 - 50 51 - 54 55 - 56
		Relativistic	57

ACKNOWLEDGEMENTS

The author expresses his sincere appreciation to Dr. P. Guyot and Mr. T. Stephansky for their numerous invaluable suggestions and contributions to this paper. He also thanks Mr. C. Cheng for his assistance with proof reading.

This research was conducted as part of the activities of the Inorganic Materials Research Division of the Lawrence Radiation Laboratory of the University of California, Berkeley, and was done under the auspices of the U. S. Atomic Energy Commission.

REFERENCES

1. N. Mott, Phil. Mag. 43, 1151 (1952).
2. A. Cottrell, J. Mech. and Phys. Sol. 1, 53 (1952).
3. A. Cottrell, Dislocations and Plastic Flow in Crystals (University Press, Oxford, 1953) p170.
4. J. Friedel, Dislocations (Pergamon Press, Oxford, 1964) pp 121, 221.
5. A. Seeger, Phil. Mag. 46, 1194 (1955).
6. F. Basinski, Phil. Mag. 4, 393 (1959).
7. A. Cottrell and B. Bilby, Proc. Phys. Soc. A62, 49 (1949).
8. N. Mott and F. Nabarro, Proc. Phys. Soc. 52, 86 (1940).
9. A. Cochardt, G. Schoeck and H. Wiedersich, Acta Met. 3, 533 (1955).
10. R. Fleischer, Acta Met. 10, 835 (1962).
11. R. Fleischer and W. Hibbard, The Relation between the Structure and Mechanical Properties of Metals (Her Majesty's Stationery Office, London, 1963) p 262.
12. J. Friedel, Dislocations (Pergamon Press, Oxford, 1964) p 351.
13. A. Kelly and M. Fine, Acta Met. 5, 365 (1957).
14. R. Fleischer, Acta Met. 8, 32 (1961).
15. M. Fine, The Relation between the Structure and Mechanical Properties of Metals (Her Majesty's Stationery Office, London, 1963) p 299.
16. J. Friedel, Dislocations (Pergamon Press, Oxford, 1964) p 376.
17. A. Seeger, Proc. Second U. N. Inter. Conf. P.U.A.E. 6, 250 (1958).
18. A. Seeger, Radiation Damage in Solids, I.A.G.A. 1, 101 (1962).

19. J. Diehl and W. Shilling, Proc. 3rd U.N. Inter. Conf. P.U.A.E., 9, 72 (1964).

20. J. Diehl, G. Seidel and L. Nieman, Phys. Stat. Sol. 11, 339 (1965); Phys. Stat. Sol. 12, 405 (1965).

21. G. Saada, Acta Met. 8, 841 (1960).

22. G. Saada, Acta Met. 9, 2 and 160 (1961).

23. P. Guyot, Acta Met. 14, 955 (1966).

24. E. Orowan, Symp. on Internal Stresses in Met. and Alloys (Inst. of Met., London, 1948) p 451.

25. E. Orowan, Disl. in Met. (A.I.M.E., New York, 1954) p 131.

26. J. Fisher, E. Hart and R. Pry, Acta Met. 336 (1953).

27. G. Taylor, Proc. Roy. Soc. L.145A, 362 (1934).

28. N. Mott, Phil. Mag. 43, 1151 (1952).

29. A. Seeger, J. Diehl, S. Mader and H. Rebstock, Phil. Mag. 2, 323 (1957).

30. R. Peierls, Proc. Phys. Soc. 52, 34 (1940).

31. A. Seeger, Phil. Mag. 1, 651 (1956).

32. J. Friedel, Electron Microscopy and Strength (Interscience Pub., 1963) p 605.

33. V. Celli, M. Kabler, T. Nimoiya and R. Thomson, Phys. Rev. 131, 58 (1963).

34. J. Dorn and S. Rajnak, Trans. AIME 230, 1052 (1964).

35. P. Guyot and J. Dorn, Cana. J. of Phys. 45,983 (1967).

36. A. Seeger, Phil. Mag. 45, 771 (1954).

37. J. Friedel, Dislocations (Pergamon Press, Oxford, 1964) p 264.

38. B. Escaig, Proc. Phys. des Disl. Toulouse (1966).

39. A. Cottrell, Phil. Mag. 43, 645 (1952).

40. J. Fisher, Trans. ASM 47, 451 (1955).

41. H. Suzuki, Sci. Rep. Res. Inst. Tohoku Univ. A4, 455 (1952).

42. J. Fisher, Acta Met. 2, 9 (1954).

43. P. Flinn, Phys. Rev. 104, 350 (1956).

44. A. Cottrell, Seminar on Relation of Properties of Microstructure (Amer. Soc. Metals, Cleveland, 1955) p 151.

45. C. Zener, Elasticity and Anelasticity of Metals (Univ. of Chicago Press, 1948) p 89.

46. J. Eshelby, Proc. Roy. Soc. L. A197, 396 (1949).

47. A. Granato and K. Lücke, J. Appl. Phys. 27, 789 (1956).

48. J. Eshelby, Proc. Roy. Soc. L. A197, 396 (1957).

49. G. Leibfried, Z. Physik 127, 344 (1950).

50. J. Eshelby, Proc. Roy. Soc. A266, 222 (1962).

51. A. Akheiser, J. Phys. USSR 1, 277 (1939).

52. W. Mason, J. Acous. Soc. Amer 32, 458 (1960).

53. W. Mason and T. Bateman, J. Acous. Soc. Amer. 36, 644 (1964).

54. W. Mason, J. Appl. Phys. 35, 2779 (1964).

55. W. Mason, Phys. Rev. 97, 557 (1955).

56. W. Mason, Phys. Rev. 143, 229 (1966).

57. F. Frank, Proc. Phys. Soc. A62, 131 (1949).

58. A. Mukherjee, J. Mote and J. Dorn, Trans. AIME, 233, 1559 (1965).

59. H. Wilsdorf and D. Kuhlman-Wilsdorf, Phys. Rev. Ltrs. 3, 170 (1959).

60. A. Keh and S. Weissman, Electron Microscopy and Strength of

Crystals (Interscience, New York, 1963) p 231.

61. W. Ferguson, A. Kumar and J. Dorn, J. Appl. Phys. to be published, 1967.

62. J. Friedel, Dislocations (Pergamon Press, Oxford, 1964) p 224.

63. J. Dorn and J. Mitchell, High-Strength Materials (John Wiley and Sons, Inc., New York, 1965) p 510.

64. A. Foreman and M. Makin, Phil. Mag. 14, 911 (1966).

65. U. Kocks, Phil. Mag. 13, 541 (1966).

66. P. Guyot and T. Stephansky, unpublished research.

67. A. Cottrell and R. Stokes, Proc. Roy. Soc., A233, 17 (1955).

68. D. Wilsdorf, Trans. AIME, 224, 1047 (1962).

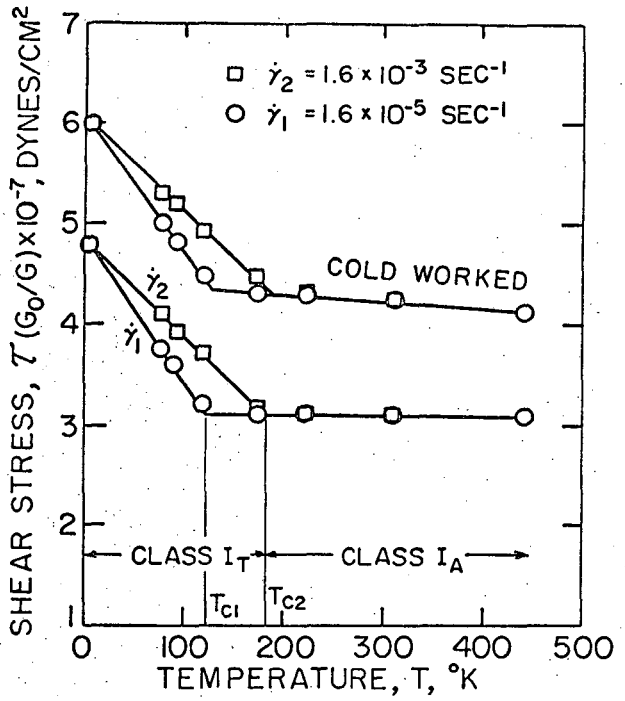

FIG. 1a. RELATIONSHIP BETWEEN STRESS, STRAIN-RATE AND TEMPERATURE FOR ALUMINUM SINGLE CRYSTALS.

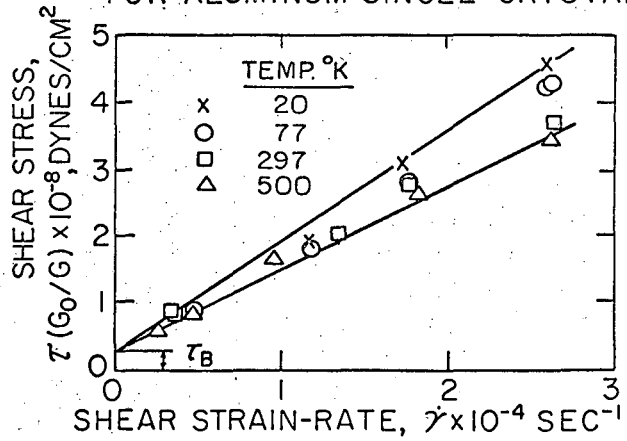

FIG. 1b. SHEAR STRESS VERSUS SHEAR STRAIN-RATE FOR DYNAMIC SHEAR IN ALUMINUM SINGLE CRYSTALS.

XBL 676-4072

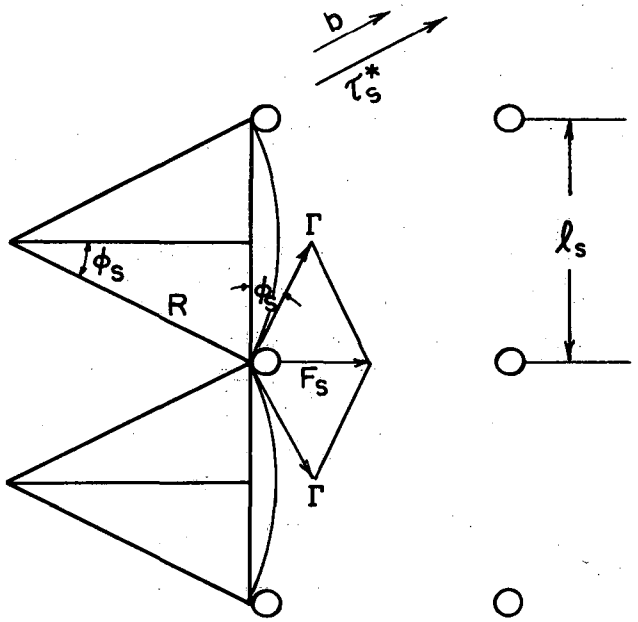

$$\tau_s^* = \frac{\Gamma}{bR}$$

$$F_s = 2\Gamma \sin \phi_s = \frac{2\Gamma \ell_s}{2R} = \tau_s^* b \ell_s$$

(a)

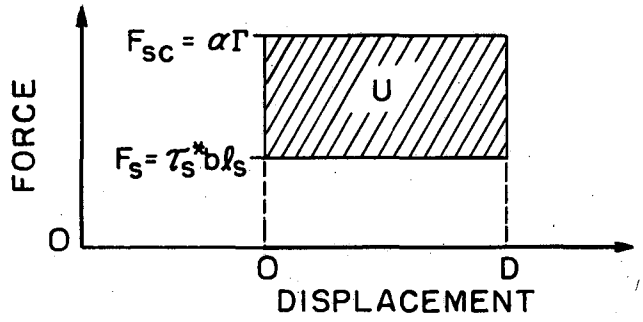

$$U = \alpha\Gamma D - \tau_s^* b \ell_s D$$

(b)

FIG. 2 PROTOTYPE FOR CUTTING.

XBL 674-1379

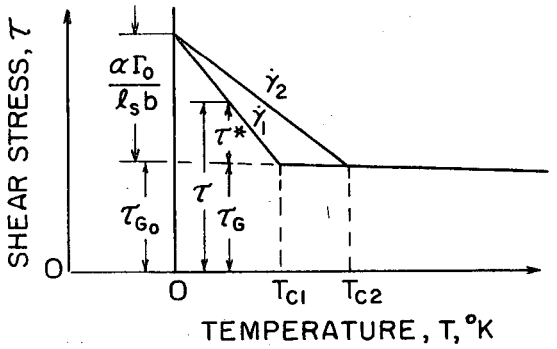

(a) EFFECT OF $\dot{\gamma}$.

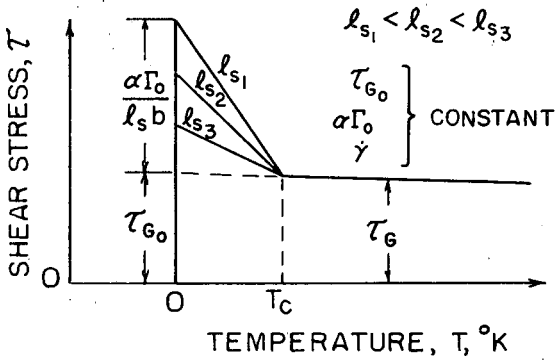

(b) EFFECT OF ℓ_s WITH NO EFFECT ON τ_G.

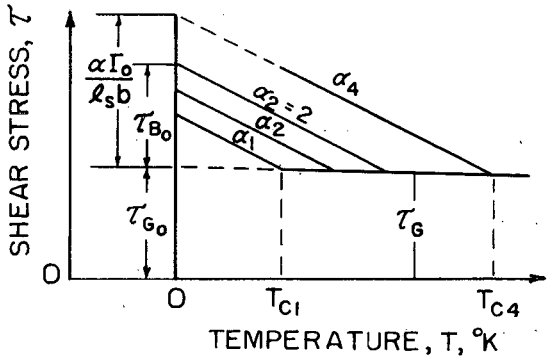

(c) INCREASING OBSTACLE STRENGTHS.

FIG. 3 SIMPLE CUTTING.

XBL 674-1380

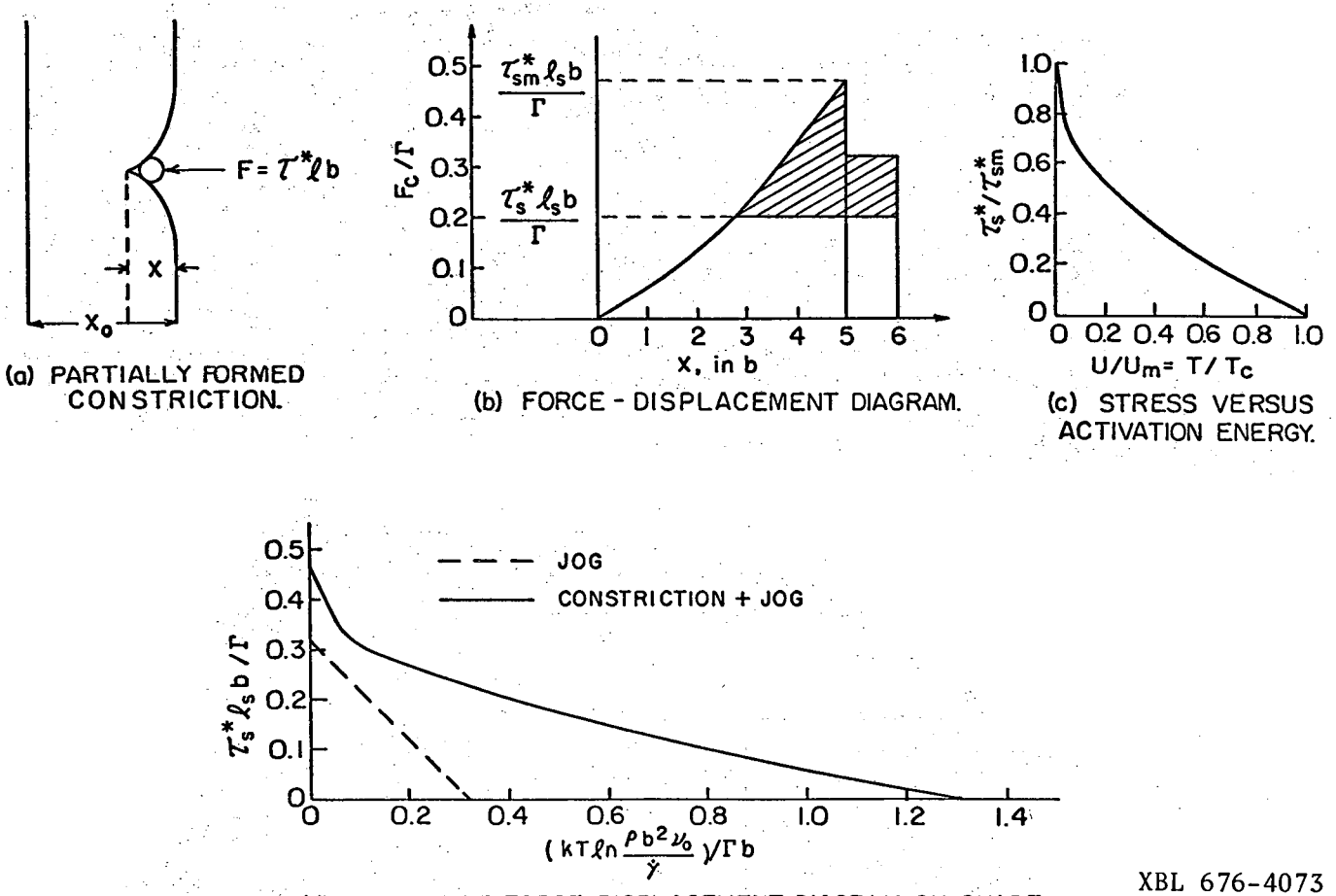

XBL 676-4073

FIG.4 CUTTING OF NONREACTIVE FOREST DISLOCATIONS BY DISSOCIATED GLIDE DISLOCATIONS.

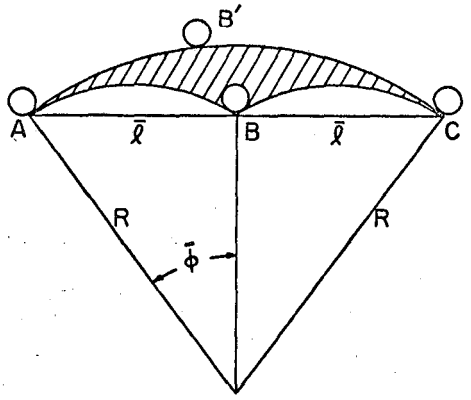

(a) AREA SWEPT OUT PER CUTTING.

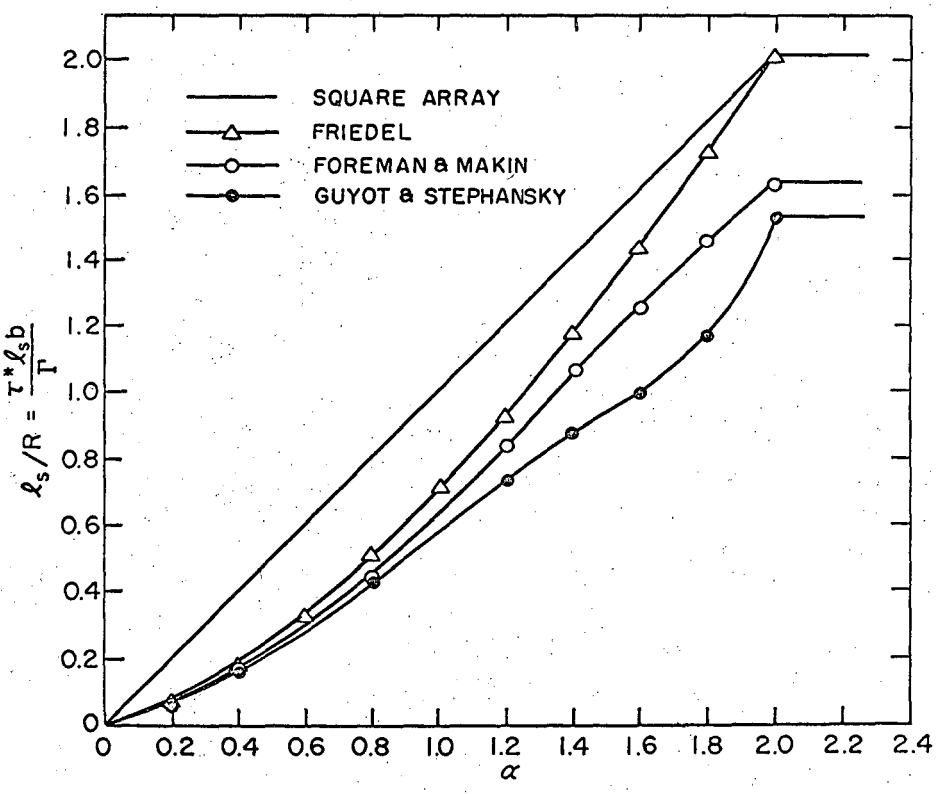

(b) ATHERMAL YIELD STRESS.

FIG. 5 EFFECT OF RANDOM DISTRIBUTION OF LOCALIZED OBSTACLES

XBL 676-4074

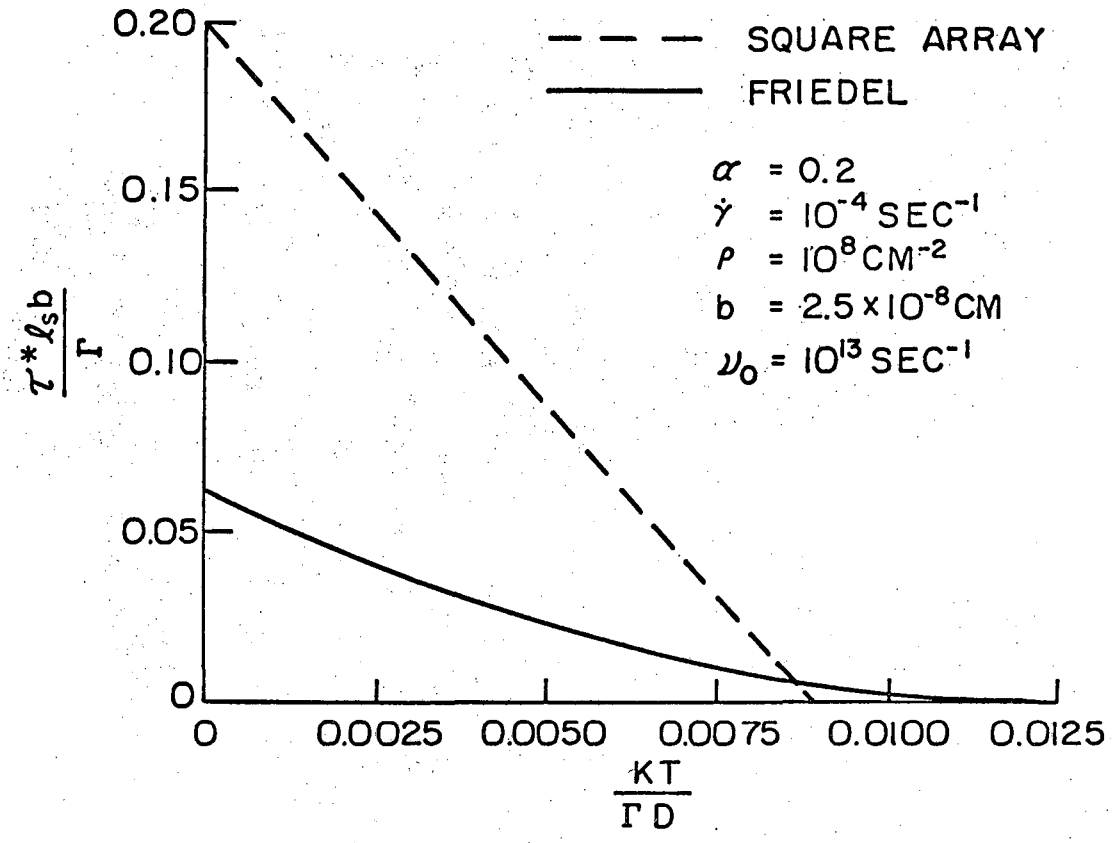

FIG. 6 COMPARISON OF PREDICTIONS BASED ON FRIEDEL'S MODEL WITH THOSE FOR A SQUARE ARRAY.

XBL 676-4075

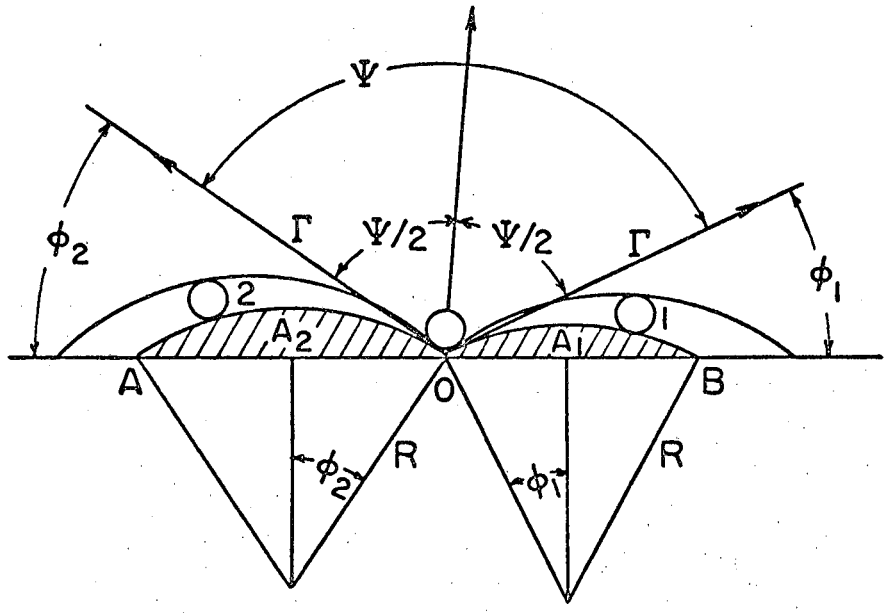

$$A_1 = R^2(\phi_1 - \sin\phi_1 \cos\phi_1) \qquad (14)$$

$$dA_1 = 2R^2 \sin^2\phi_1 \, d\phi_1 \qquad (15)$$

$$F = 2\Gamma \cos\frac{\Psi}{2} = 2\Gamma \sin\left(\frac{\phi_1+\phi_2}{2}\right) \qquad (16)$$

$$F_c = \alpha\Gamma = 2\Gamma \cos\frac{\Psi_c}{2} = 2\Gamma \sin\phi_c \qquad (17)$$

FIG. 7 FORCE ON AN OBSTACLE.

XBL 676-4076

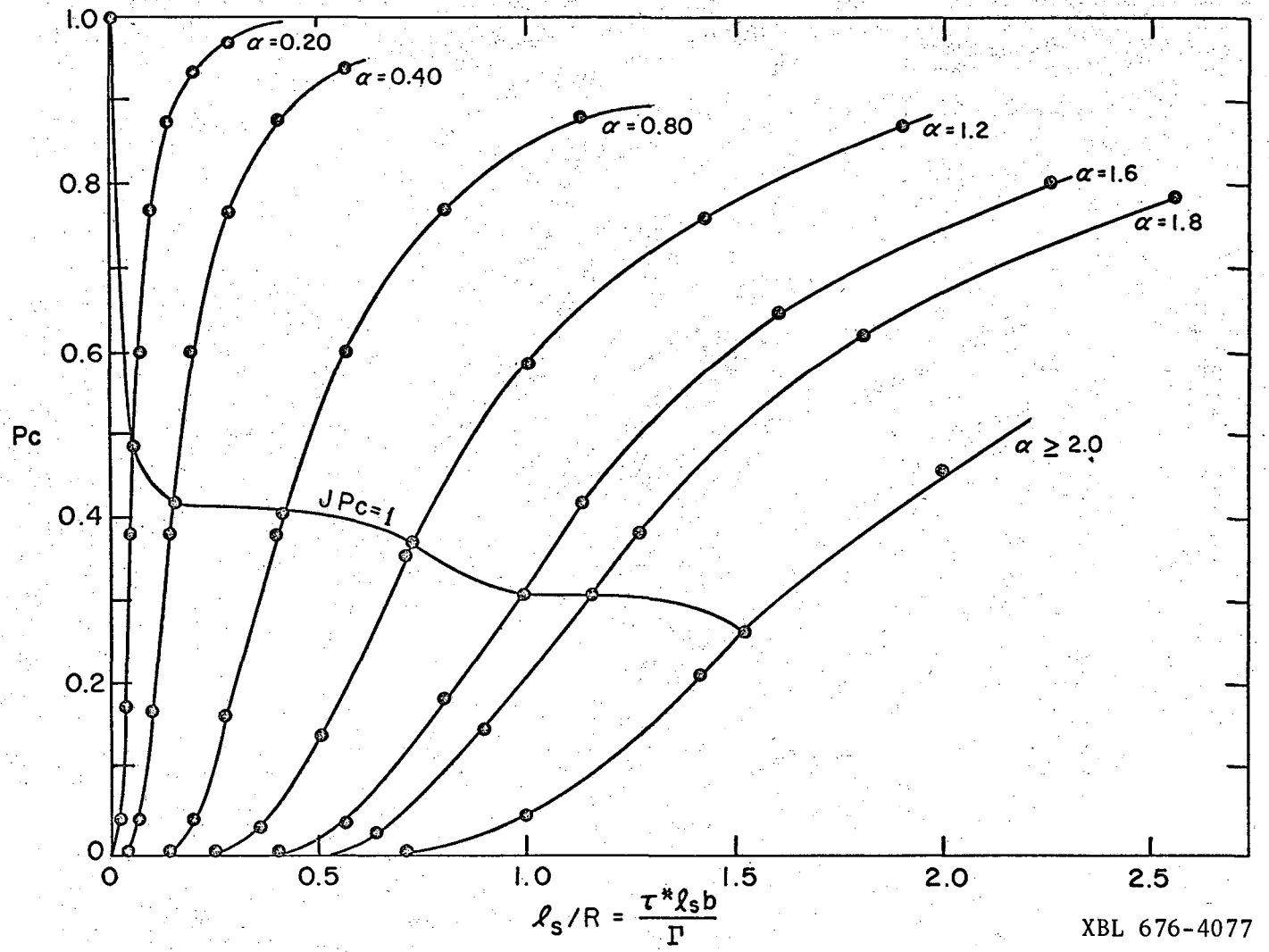

FIG. 8 PROBABILITY FOR CUTTING AND CONDITION FOR MACROSCOPIC YIELDING.

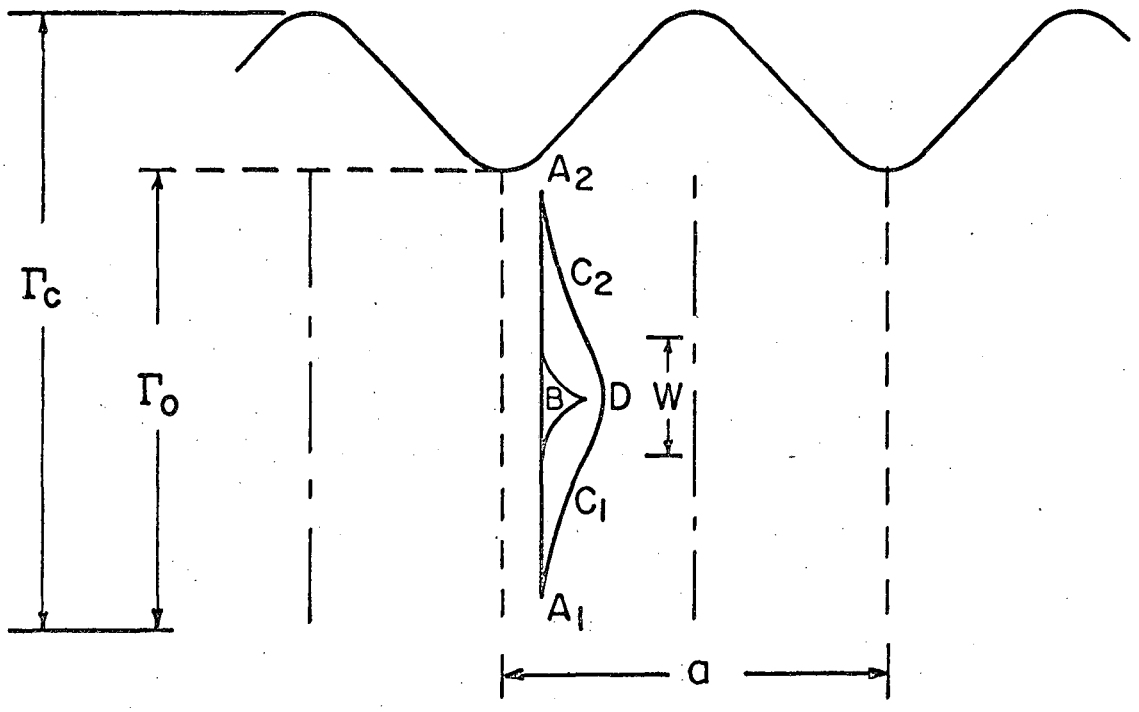

(a) NUCLEATION OF KINKS.

XBL 676-4078

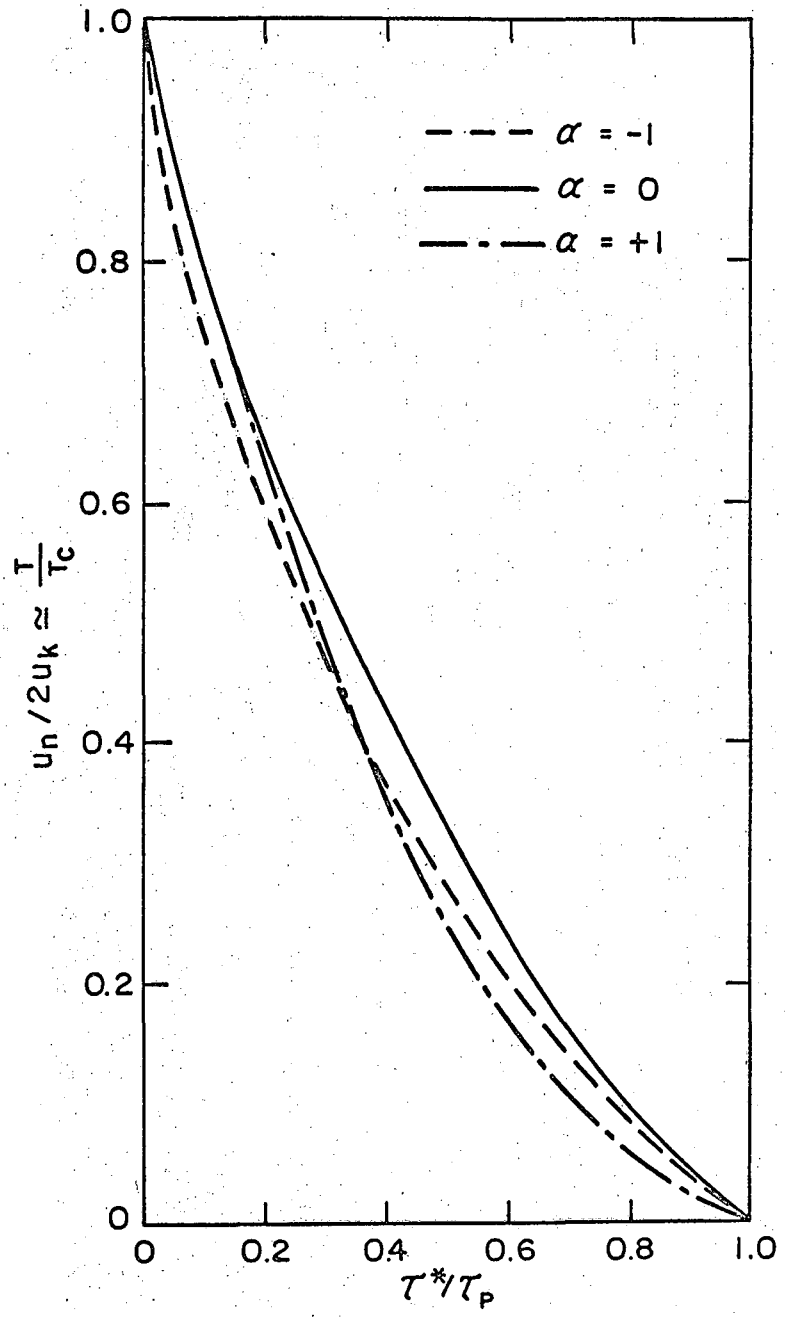

(b) ACTIVATION ENERGY.

XBL 676-4079

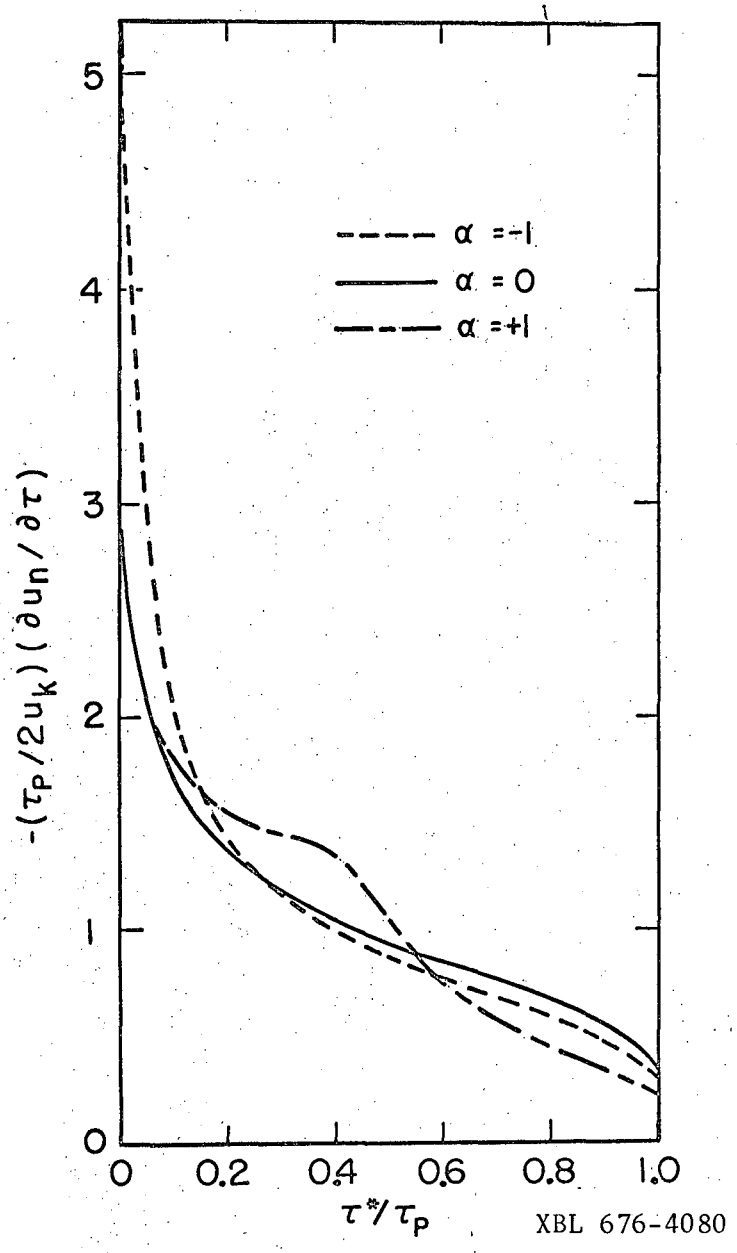

(c) ACTIVATION VOLUME.

FIG. 9 PEIERLS MECHANISM.

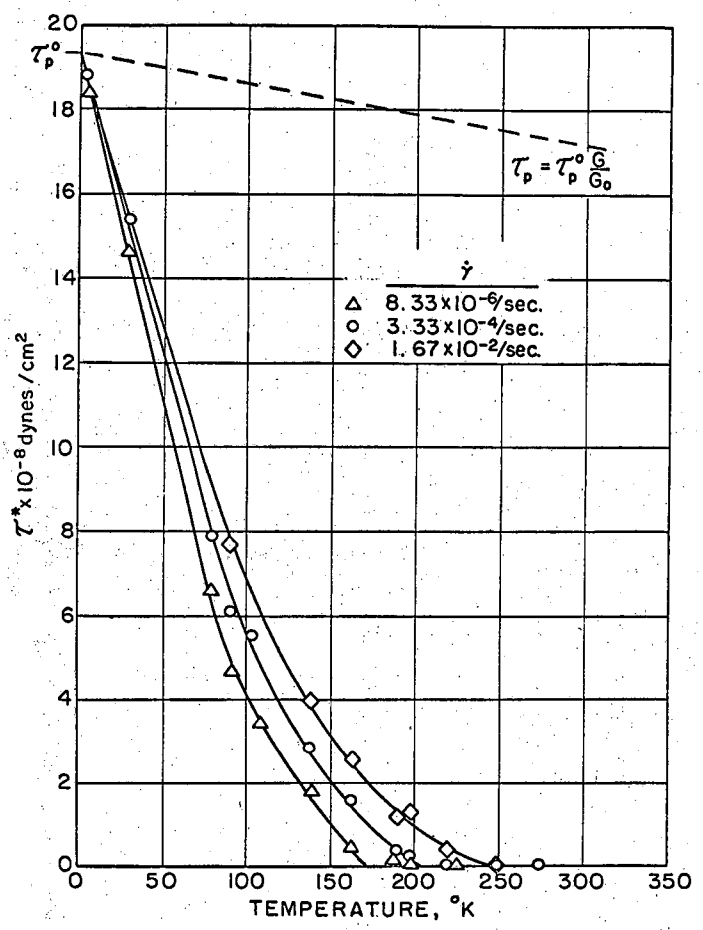

FIG. 10 a. THE THERMALLY ACTIVATED COMPONENT OF THE FLOW STRESS vs. TEMPERATURE FOR DIFFERENT STRAIN RATES.

XBL 676-4081

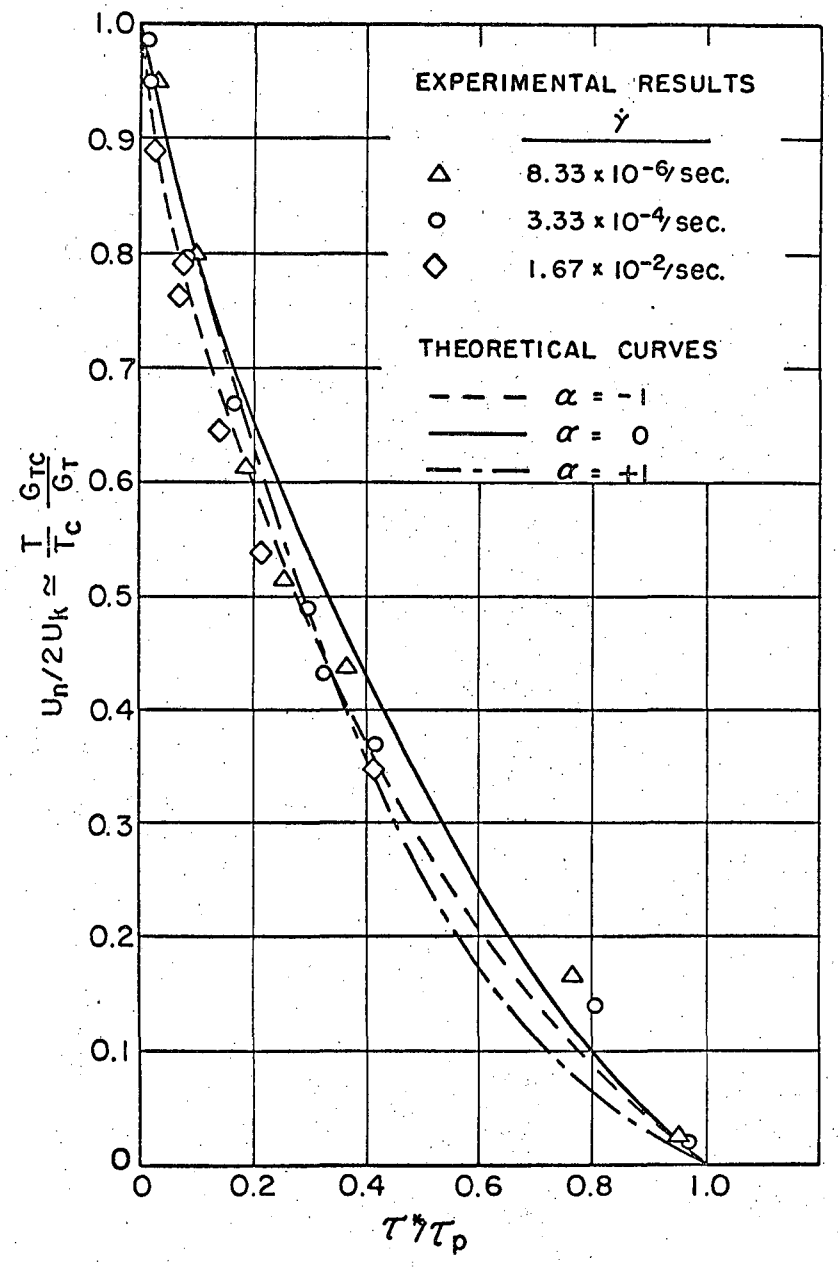

FIG. 10 b. THE THERMALLY ACTIVATED COMPONENT OF THE FLOW STRESS vs. TEMPERATURE IN DIMENSIONLESS UNITS.

XBL 676-4082

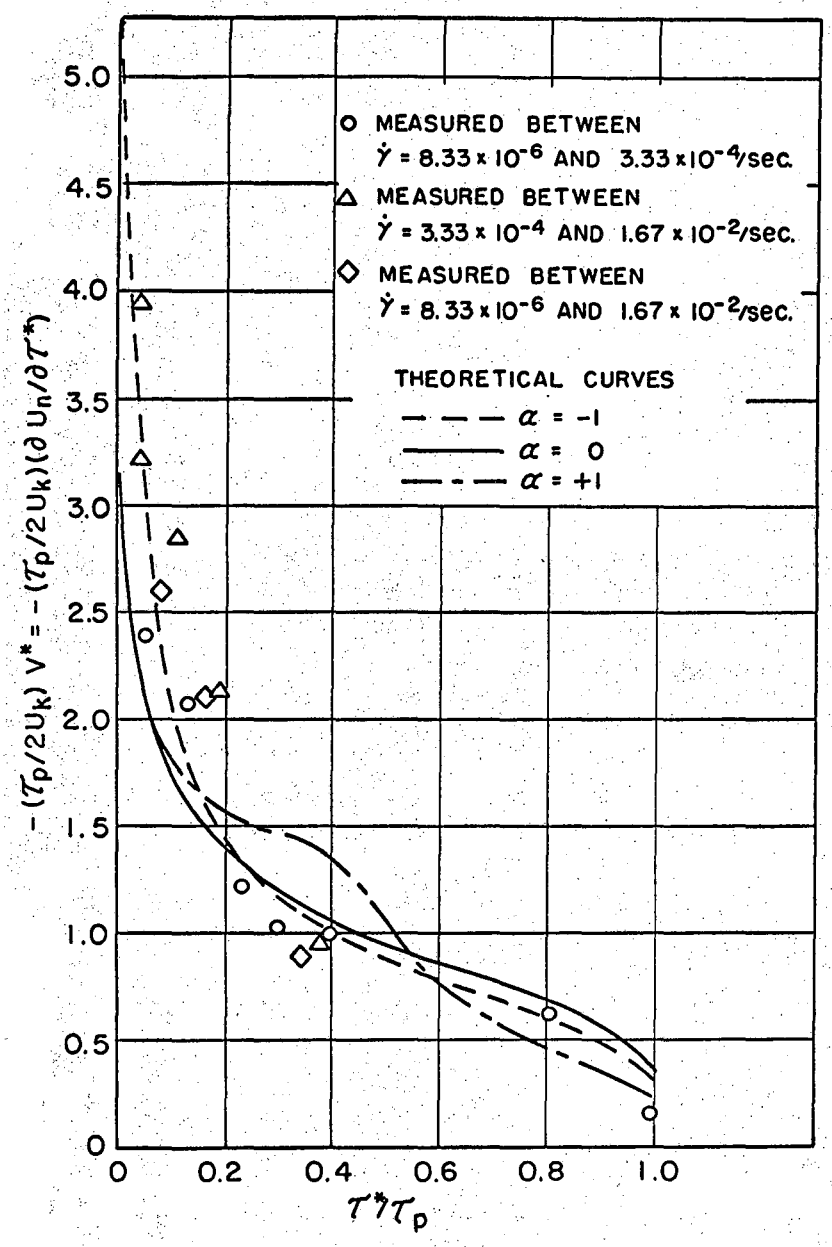

FIG. 10c. THE THERMALLY ACTIVATED COMPONENT OF THE FLOW STRESS vs. THE ACTIVATION VOLUME IN-DIMENSIONLESS UNITS.

XBL 676-4083

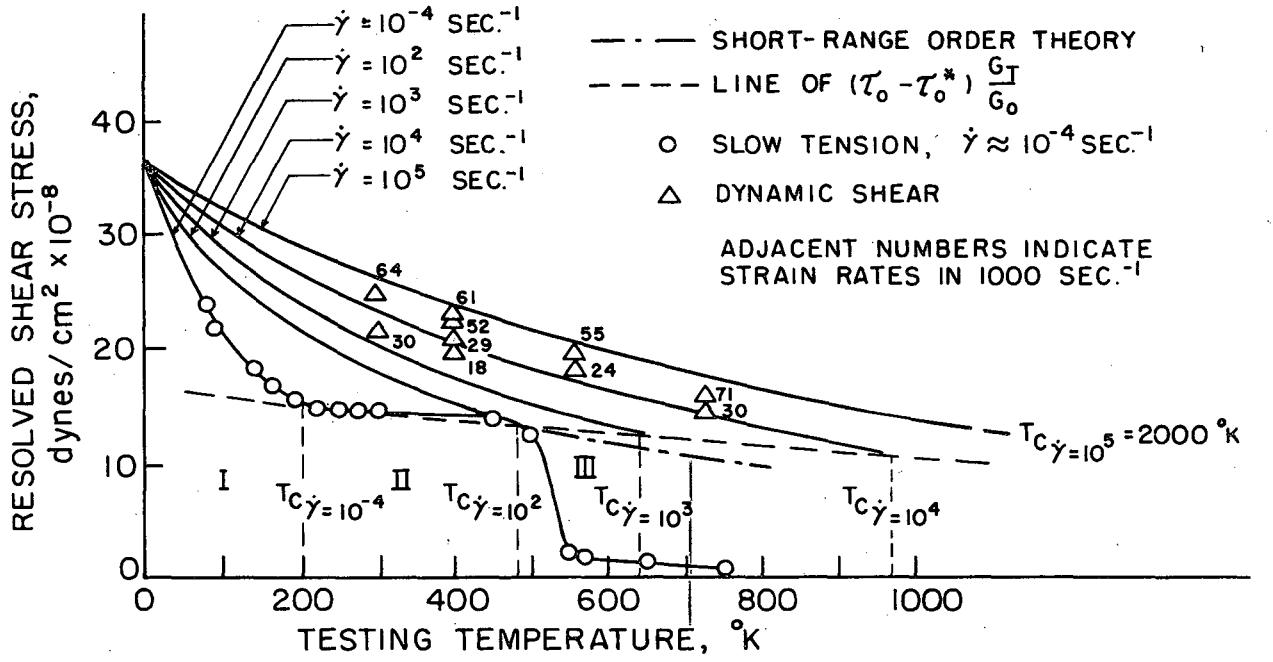

FIG.10d RESOLVED SHEAR STRESS vs. TEMPERATURE FOR PRISMATIC SLIP IN Ag_2 - Al.

MUB-3113

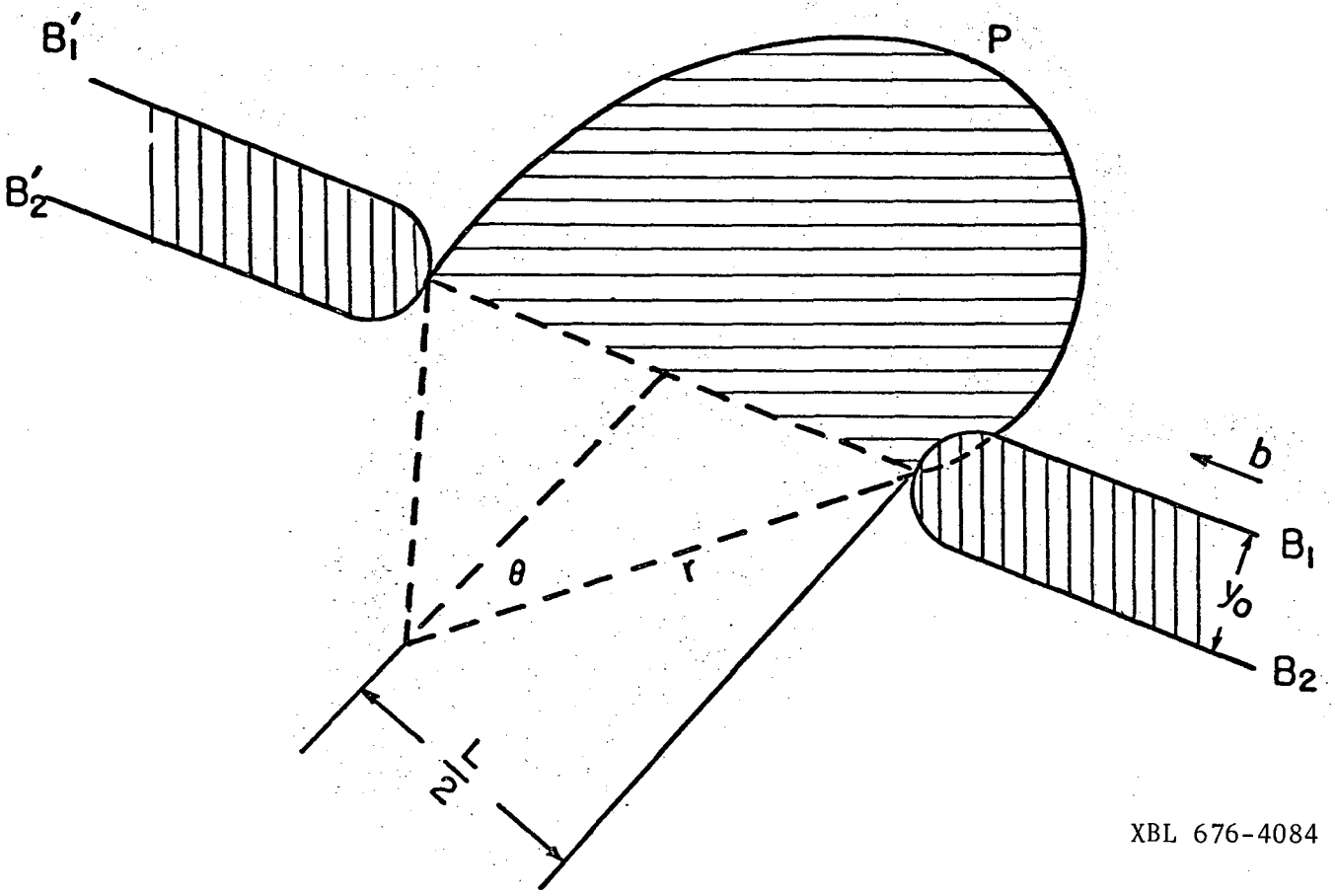

XBL 676-4084

FIG. 11 NUCLEATION OF CROSS SLIP AS A RESULT OF RECOMBINATION OF THE PARTIALS B_1 AND B_2 ON THE BASAL PLANE ALONG LENGTH L AND BOWING OUT OF THE RECOMBINED SECTION P ON THE PRISM PLANE.

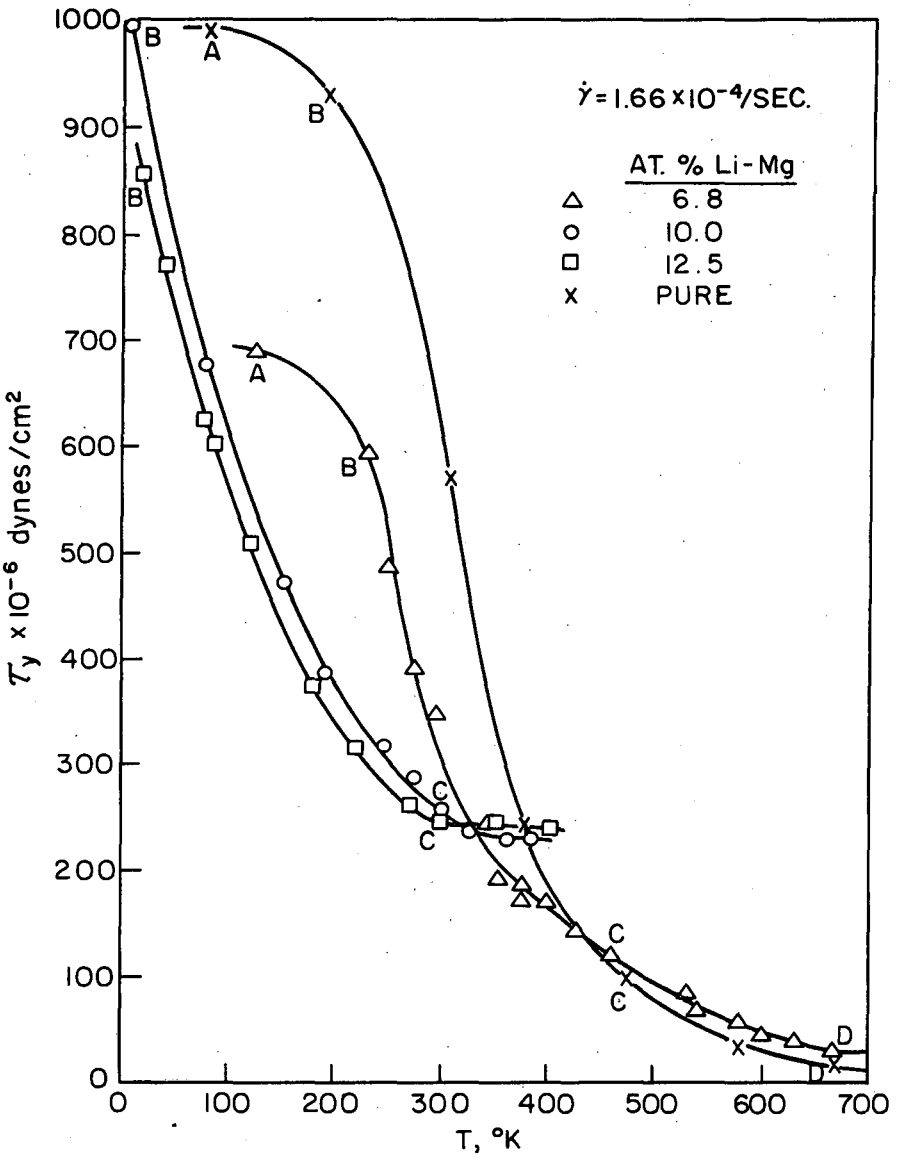

FIG. 12 CRITICAL RESOLVED SHEAR STRESS vs. TEMPERATURE FOR PRISMATIC SLIP IN PURE Mg AND Li-Mg ALLOYS.

MUB-3121